

# Uniform Bounds with Difference Quotients for Proper Orthogonal Decomposition Reduced Order Models of the Burgers Equation

Birgul Koc <sup>\*</sup>, Tomás Chacón Rebollo <sup>†</sup>, Samuele Rubino <sup>‡</sup>

## Abstract

In this paper, we work uniform error bounds for proper orthogonal decomposition reduced order modeling (POD-ROM) of Burgers equation, considering difference quotients (DQs), introduced in [23]. In particular, we study the optimality behavior of the DQ ROM error bounds by considering  $L^2(\Omega)$  and  $H_0^1(\Omega)$  POD spaces. We present some meaningful numerical tests checking the optimality error behavior. Based on our numerical observations, noDQ POD-ROM errors have an optimal behavior, while DQ POD-ROM errors demonstrate an optimality/super-optimality behavior. It is conjectured that this possibly occurs because the DQ inner products allow the time dependency in the ROM spaces to take into account.

**Keywords:** Difference Quotients, Proper Orthogonal Decomposition, Reduced Order Models, Error Analysis, Optimality.

## 1 Introduction

Reduced order models (ROMs) are one of the most popular low-dimensional surrogate models to obtain the numerical simulation of linear and nonlinear systems [10, 13, 15–18, 22, 31–34, 41–43]. To build a low dimensional ROM, one can use the following most popular frameworks such as proper orthogonal decomposition (POD) [1, 3–7, 12, 14, 17, 20, 24, 30, 32, 44, 45], reduced basis methods (RBM) [8, 35, 39], empirical interpolation method (EIM), and discrete empirical interpolation method (DEIM) [2, 11, 36, 38]. In this work, we specifically use the POD framework to build the ROM.

The POD-ROM error analysis for the parabolic problems has been worked in [19, 25, 27, 29, 40]. *Difference quotients (DQs)* (i.e., scaled snapshots of the form  $(u^n - u^{n-1})/\Delta t$ ,  $n = 1, \dots, N$ ) proposed by Kunisch and Volkwein in Remark 1 of [26] as a means to achieve time discretization optimality. The effect of the DQs in linear applications and in the POD-ROM error analysis for the parabolic problems is investigated in [9, 28] and [19, 21, 25, 29], respectively. The authors in [19] provide the DQ POD-ROM errors for the Burgers equation without providing any numerical analysis for the results. Thus, we emphasize that, to our knowledge, the POD-ROM error analysis considering the DQs for the nonlinear problems has never been proved.

The main aim of the paper is to provide uniform POD-ROM error bounds for the Burgers equation (1) considering DQ,  $L^2(\Omega)$  and  $H_0^1(\Omega)$  POD space frameworks and the

---

<sup>\*</sup>Departamento IMUS, Universidad de Sevilla, Spain. [birkoc@alum.us.es](mailto:birkoc@alum.us.es)

<sup>†</sup>Departamento EDAN & IMUS, Universidad de Sevilla, Spain. [chacon@us.es](mailto:chacon@us.es)

<sup>‡</sup>Departamento EDAN & IMUS, Universidad de Sevilla, Spain. [samuele@us.es](mailto:samuele@us.es)

$l^\infty(L^2(\Omega))$  and natural-norms. The rest of the paper is organized as follows: In Section 2, we briefly describe the noDQ/DQ POD methodology and provide error bounds for the POD projection error. The error analysis for the DQ Crank-Nicolson POD-ROM (DQ CN-POD-ROM) for the Burgers equation (1) is presented in Section 3. Specifically, in Sections 4.1 and 4.2, we provide  $l^\infty(L^2)$  and natural-norm, i.e.,  $l^\infty(L^2) \cap l^2(H_0^1)$  DQ CN-POD-ROM error bounds considering  $L^2(\Omega)$  and  $H_0^1(\Omega)$  POD bases and their optimality behavior, respectively.

$$\begin{cases} u_t - \nu u_{xx} + uu_x = f, & x \in \Omega, t \in (0, T), \\ u(0, t) = u(1, t) = 0, & t \in (0, T), \\ u(x, 0) = u_0(x), & x \in \Omega. \end{cases} \quad (1)$$

Furthermore, in Sections 5.0.1 and 5.0.2, we numerically discuss the optimality behavior of the  $l^\infty(L^2)$  and natural norm DQ CN-POD-ROM errors considering  $L^2(\Omega)$  and  $H_0^1(\Omega)$  POD bases. In Section 5.0.3, we numerically compare and discuss the noDQ and DQ CN-POD-ROM errors considering both POD spaces and norm errors. Finally, Section 6 presents the conclusions and future research directions.

## 2 Proper Orthogonal Decomposition (POD)

This section draws a general POD framework with/without DQs. The construction of the noDQ/DQ POD basis is straightforward and can be summarized in the following steps: (i) We collect snapshots data set  $\{u_h^0, u_h^1, \dots, u_h^N\}$  that is contained in a real Hilbert space  $\mathcal{H}$  and solves the problem (1) for different parameter  $t_0, t_1, \dots, t_N$ , respectively. (ii) We obtain noDQ/DQ orthonormal POD basis functions (usually called POD modes), i.e.,  $\{\varphi_1, \dots, \varphi_r\} \in \mathcal{H}$  with fixed  $r > 0$  value by solving the following minimization problem:

$$\min_{(\varphi_i, \varphi_j)_{\mathcal{H}} = \delta_{ij}} \|u_h - P_r u_h\|_*^2 \quad (2)$$

where the  $*$  norm is defined as

$$\|v\|_* := \frac{1}{\sqrt{M}} \left( \sum_{i=0}^N \|v^i\|_{\mathcal{H}}^2 + \sum_{i=1}^N \|\partial v^i\|_{\mathcal{H}}^2 \right)^{1/2}, \quad (3)$$

being the weight  $M = 2N + 1$  and the DQs, i.e.,  $\partial v^k$ , defined by

$$\partial v^k := \frac{v^k - v^{k-1}}{\Delta t}, \quad (4)$$

and  $P_r : \mathcal{H} \rightarrow \mathcal{H}$  is the orthogonal projection onto  $X^r := \text{span}\{\varphi_i\}_{i=1}^r$  given by

$$P_r u_h = \sum_{i=1}^r (u_h, \varphi_i)_{\mathcal{H}} \varphi_i, \quad u_h \in \mathcal{H}. \quad (5)$$

If one discards the second summation in (3), which contains the DQs, and chooses the weight  $M = N + 1$  in (3), then the minimization problem (2) is solved to obtain the standard POD (noDQ POD) basis. Furthermore, the Hilbert space  $\mathcal{H}$  is chosen as either  $L^2$  or  $H_0^1$  in (3) to obtain the DQ L2-POD and H01-POD space framework, respectively.

Now, we provide DQ POD-ROM approximation errors in Lemma 2.1 proven in [19] by considering different norms and projections onto  $X^r$ . Furthermore, we present the uniform DQ POD-ROM projection error bounds in Theorem 2.2 proved in ([23], Theorem 3.7). These results are necessary to prove DQ POD-ROM error bounds and show their optimality behavior in Section 3.

**Lemma 2.1.** Let  $X^r = \text{span}\{\varphi_i\}_{i=1}^r \subset \mathcal{H}$ , let  $P_r : \mathcal{H} \rightarrow \mathcal{H}$  be the orthogonal projection onto  $X^r$  as defined in (5), and let  $d$  be the number of positive POD eigenvalues for the collection  $U^{\text{DQ}} = \{u_h^n\}_{n=0}^N \cup \{\partial u_h^n\}_{n=1}^N$  described above. If  $W$  is a real Hilbert space with  $U^{\text{DQ}} \subset W$  and  $R_r : W \rightarrow W$  is a bounded linear projection onto  $X^r$ , then

$$\frac{1}{2N+1} \left( \sum_{n=0}^N \|u_h^n - P_r u_h^n\|_W^2 + \sum_{n=1}^N \|\partial u_h^n - P_r \partial u_h^n\|_W^2 \right) = \sum_{i=r+1}^d \lambda_i^{\text{DQ}} \|\varphi_i\|_W^2, \quad (6a)$$

$$\frac{1}{2N+1} \left( \sum_{n=0}^N \|u_h^n - R_r u_h^n\|_W^2 + \sum_{n=1}^N \|\partial u_h^n - R_r \partial u_h^n\|_W^2 \right) = \sum_{i=r+1}^d \lambda_i^{\text{DQ}} \|\varphi_i - R_r \varphi_i\|_W^2. \quad (6b)$$

**Theorem 2.2.** Let  $X^r = \text{span}\{\varphi_i\}_{i=1}^r \subset \mathcal{H}$ , let  $P_r : \mathcal{H} \rightarrow \mathcal{H}$  be the orthogonal projection onto  $X^r$  as defined in (5), and let  $d$  be the number of positive POD eigenvalues for  $U^{\text{DQ}}$ . If  $W$  is a real Hilbert space with  $U^{\text{DQ}} \subset W$  and  $R_r : W \rightarrow W$  is a bounded linear projection onto  $X^r$ , then

$$\max_{0 \leq k \leq N} \|u_h^k - P_r u_h^k\|_{\mathcal{H}}^2 \leq C \sum_{i=r+1}^d \lambda_i^{\text{DQ}}, \quad (7a)$$

$$\max_{0 \leq k \leq N} \|u_h^k - P_r u_h^k\|_W^2 \leq C \sum_{i=r+1}^d \lambda_i^{\text{DQ}} \|\varphi_i\|_W^2, \quad (7b)$$

$$\max_{0 \leq k \leq N} \|u_h^k - R_r u_h^k\|_W^2 \leq C \sum_{i=r+1}^s \lambda_i^{\text{DQ}} \|\varphi_i - R_r \varphi_i\|_W^2, \quad (7c)$$

where  $C = 6 \max\{1, T^2\}$ .

**Remark 2.3.** The bounds in Lemma 2.1 and Theorem 2.2 are still valid if one replaces the snapshots data  $\{u_h^0, u_h^1, \dots, u_h^N\}$  which are finite element (FE) solutions in this paper with the continuous solution data  $\{u^0, u^1, \dots, u^N\}$ . Furthermore, the data set which is used to generate the POD basis in (2) should be the same as the data set is used in the POD projection error bounds in Lemma 2.1 and Theorem 2.2.

### 3 Reduced Order Modeling (ROM)

In this section, we present a numerical method for the Burgers equation (1), which is the proper orthogonal decomposition reduced order model (POD-ROM).

First, we define the function space  $X = H_0^1(\Omega)$  endowed with the inner product  $(u, v)_{H_0^1} = (u_x, v_x)_{L^2}$ . We take  $u(\cdot, t) \in X$ ,  $t \in [0, T]$  to be the weak solution of the weak formulation of the Burgers equation with homogeneous Dirichlet boundary conditions:

$$(\partial_t u, v)_{L^2} + \nu(u_x, v_x)_{L^2} + (u u_x, v)_{L^2} = (f, v)_{L^2} \quad \forall v \in X. \quad (8)$$

We assume that  $u$  is smooth enough to have  $\partial_t u \in L^2(0, T; L^2(\Omega))$ . Applying Crank-Nicolson and Galerkin discretizations in time and space, respectively to the weak formulation of the Burgers equation (8) results in the CN-POD-ROM:  $\forall v_r \in X^r$ ,

$$(\partial u_r^{n+1}, v_r)_{L^2} + \nu((u_r)_x^{n+1/2}, (v_r)_x)_{L^2} + (u_r^{n+1/2}(u_r)_x^{n+1/2}, v_r)_{L^2} = (f^{n+1/2}, v_r)_{L^2}, \quad (9)$$

where  $\partial u_r^{n+1} := (u_r^{n+1} - u_r^n)/\Delta t$ .

**Remark 3.1.** We use the notation  $z^{n+1/2}$  for any discrete-time function  $z$  to denote the average  $z^{n+1/2} := \frac{1}{2}(z^{n+1} + z^n)$ . However, for a continuous time function, we use  $f^{n+1/2}$  to denote  $f(t_n + \Delta t/2)$ .

## 4 Error Analysis

In this section, we prove uniform error bounds for the DQ CN-POD-ROM for the Burgers equation (1). Specifically, we provide  $l^\infty(L^2)$  and natural-norm ( $l^\infty(L^2) \cap l^2(H_0^1)$ ) error bounds considering  $L^2(\Omega)$  and  $H_0^1(\Omega)$  POD bases and their optimality behavior in Section 4.1 and Section 4.2, respectively.

We start the analysis by applying the CN time discretization to (8), which yields the following:  $\forall v \in X$ ,

$$(\partial u^{n+1}, v)_{L^2} + \nu(u_x^{n+1/2}, v_x)_{L^2} + (u^{n+1/2}u_x^{n+1/2}, v)_{L^2} = (f^{n+1/2}, v)_{L^2} + \tau_n(v), \quad (10)$$

with the corresponding consistency error

$$\begin{aligned} \tau_n(v) := & (\partial u^{n+1} - \partial_t u(t_n + \Delta t/2), v)_{L^2} + \nu \left( u_{xx}(t_n + \Delta t/2) - u_x^{n+1/2}, v \right)_{L^2} \\ & + \left( u^{n+1/2}u_x^{n+1/2} - u(t_n + \Delta t/2)u_x(t_n + \Delta t/2), v \right)_{L^2}. \end{aligned} \quad (11)$$

The consistency error (11) does not depend on the  $f$  term because of Remark 3.1. Furthermore, we assume the following regularity conditions on the continuous solution  $u$  and the terms in (11):

$$u \in L^\infty(H_0^1(\Omega)), \quad (12a)$$

$$u_{ttt}, (u_{tt})_{xx}, (u(u_{tt})_x + u_{tt}u_x) \in L^2(0, T; L^2(\Omega)). \quad (12b)$$

Now, we define the regularity constants, which are the bounds for the terms in (12b) as

$$\begin{aligned} I_{n,1}(u) := & \|u_{ttt}\|_{L^2(t_n, t_{n+1}; L^2)} + \|(u_{tt})_{xx}\|_{L^2(t_n, t_{n+1}; L^2)} \\ & + \|u(u_{tt})_x + u_{tt}u_x\|_{L^2(t_n, t_{n+1}; L^2)}, \\ I_n(u) := & \|u_{ttt}\|_{L^2(t_n, t_{n+1}; L^2)}^2 + \|(u_{tt})_{xx}\|_{L^2(t_n, t_{n+1}; L^2)}^2 \\ & + \|u(u_{tt})_x + u_{tt}u_x\|_{L^2(t_n, t_{n+1}; L^2)}^2, \\ I(u) := & \|u_{ttt}\|_{L^2(0, T; L^2)}^2 + \|(u_{tt})_{xx}\|_{L^2(0, T; L^2)}^2 \\ & + \|u(u_{tt})_x + u_{tt}u_x\|_{L^2(0, T; L^2)}^2. \end{aligned} \quad (13)$$

Now, we subtract (9) from (10) by choosing  $v = v_r$  in (10) (since  $X^r \subset X$ ), and label the discretized error  $e^{n+1} := u^{n+1} - u_r^{n+1}$ . Then, one gets the following error equation:  $\forall v_r \in X^r$ ,

$$\begin{aligned} & (\partial e^{n+1}, v_r)_{L^2} + \nu(e_x^{n+1/2}, (v_r)_x)_{L^2} + (u^{n+1/2}u_x^{n+1/2}, v_r)_{L^2} \\ & - (u_r^{n+1/2}(u_r)_x^{n+1/2}, v_r)_{L^2} = \tau_n(v_r). \end{aligned} \quad (14)$$

Then, we split the discretized error  $e^{n+1}$  into two parts as

$$\begin{aligned} e^{n+1} = u^{n+1} - u_r^{n+1} &= (u^{n+1} - w_r^{n+1}) - (u_r^{n+1} - w_r^{n+1}) \\ &= \eta^{n+1} - \phi_r^{n+1}, \end{aligned} \quad (15)$$

where  $w_r^{n+1} := R_r u^{n+1}$  is chosen as a Ritz projection of  $u^{n+1}$  on  $X^r$  (for different analyses,  $w_r$  could be chosen differently), which is defined as

$$((u - R_r u)_x, (v_r)_x)_{L^2} = 0 \quad \forall v_r \in X^r, \quad (16)$$

$\eta^{n+1} := u^{n+1} - w_r^{n+1}$  is the POD projection error and  $\phi_r^{n+1} := u_r^{n+1} - w_r^{n+1}$  is the discretization error. During the analysis, we need a standard stability estimate of  $u_r^n$  for the CN scheme, which is

$$\max_{0 \leq n \leq N} \|u_r^n\|_{L^2} \leq C. \quad (17)$$

Now, by using the error splitting (15), one can rewrite the error equation (14) as

$$\begin{aligned} (\partial\phi_r^{n+1}, v_r)_{L^2} + \nu((\phi_r)_x^{n+1/2}, (v_r)_x)_{L^2} &= (\partial\eta^{n+1}, v_r)_{L^2} + \nu(\eta_x^{n+1/2}, (v_r)_x)_{L^2} \\ &\quad + (u^{n+1/2}u_x^{n+1/2}, v_r)_{L^2} - (u_r^{n+1/2}(u_r)_x^{n+1/2}, v_r)_{L^2} - \tau_n(v_r). \end{aligned} \quad (18)$$

Then, (16) leads to  $(\eta_x, (v_r)_x)_{L^2} = 0$ ,  $\forall v_r \in X^r$ ; thus, the second term  $(\eta_x^{n+1/2}, (v_r)_x)_{L^2}$  on the right-hand side of (18) vanishes. We continue the error analysis by choosing  $v_r := \phi_r^{n+1/2}$ , then (18) is rewritten as

$$\begin{aligned} \frac{1}{2\Delta t} \left( \|\phi_r^{n+1}\|_{L^2}^2 - \|\phi_r^n\|_{L^2}^2 \right) + \nu \|(\phi_r)_x^{n+1/2}\|_{L^2}^2 &= (\partial\eta^{n+1}, \phi_r^{n+1/2})_{L^2} \\ &\quad + (u^{n+1/2}u_x^{n+1/2}, \phi_r^{n+1/2})_{L^2} - (u_r^{n+1/2}(u_r)_x^{n+1/2}, \phi_r^{n+1/2})_{L^2} - \tau_n(\phi_r^{n+1/2}). \end{aligned} \quad (19)$$

Now, we individually bound the terms in (19). During the analysis,  $C$  is a generic constant that only depends on the data. By using the Cauchy-Schwarz inequality and the Young's inequality, the first term on the right-hand side of (19), can be bounded as

$$\begin{aligned} (\partial\eta^{n+1}, \phi_r^{n+1/2})_{L^2} &\leq \|\partial\eta^{n+1}\|_{L^2} \|\phi_r^{n+1/2}\|_{L^2} \\ &\leq \frac{1}{4} \|\partial\eta^{n+1}\|_{L^2}^2 + \|\phi_r^{n+1/2}\|_{L^2}^2. \end{aligned} \quad (20)$$

Next, we arrange the nonlinear terms in (19) by adding and subtracting the term  $(u_r^{n+1/2}u_x^{n+1/2}, \phi_r^{n+1/2})_{L^2}$ . Then, we rewrite the nonlinear terms as

$$\begin{aligned} &(u^{n+1/2}u_x^{n+1/2}, \phi_r^{n+1/2})_{L^2} - (u_r^{n+1/2}(u_r)_x^{n+1/2}, \phi_r^{n+1/2})_{L^2} \\ &= ((u - u_r)^{n+1/2}u_x^{n+1/2}, \phi_r^{n+1/2})_{L^2} + (u_r^{n+1/2}(u - u_r)_x^{n+1/2}, \phi_r^{n+1/2})_{L^2} \\ &= (\eta^{n+1/2}u_x^{n+1/2}, \phi_r^{n+1/2})_{L^2} - (\phi_r^{n+1/2}u_x^{n+1/2}, \phi_r^{n+1/2})_{L^2} \\ &\quad + (u_r^{n+1/2}\eta_x^{n+1/2}, \phi_r^{n+1/2})_{L^2} - (u_r^{n+1/2}(\phi_r)_x^{n+1/2}, \phi_r^{n+1/2})_{L^2}. \end{aligned} \quad (21)$$

Now, we individually bound nonlinear terms in (21). By using the Hölder's inequality, the regularity condition of the continuous solution in (12a), and Young's inequality, we can bound the first term in (21) as

$$\begin{aligned} (\eta^{n+1/2}u_x^{n+1/2}, \phi_r^{n+1/2})_{L^2} &\leq \|\eta^{n+1/2}\|_{L^2} \|u_x^{n+1/2}\|_{L^\infty} \|\phi_r^{n+1/2}\|_{L^2} \\ &\leq C \|\eta^{n+1/2}\|_{L^2} \|\phi_r^{n+1/2}\|_{L^2} \\ &\leq C \|\eta^{n+1/2}\|_{L^2}^2 + \|\phi_r^{n+1/2}\|_{L^2}^2. \end{aligned} \quad (22)$$

For the second term in (21), we use the Hölder's inequality and the regularity condition of the continuous solution in (12a) as

$$\begin{aligned} (\phi_r^{n+1/2}u_x^{n+1/2}, \phi_r^{n+1/2})_{L^2} &\leq \|\phi_r^{n+1/2}\|_{L^2} \|u_x^{n+1/2}\|_{L^\infty} \|\phi_r^{n+1/2}\|_{L^2} \\ &\leq C \|\phi_r^{n+1/2}\|_{L^2}^2. \end{aligned} \quad (23)$$

For the third term in (21), we use the Hölder's inequality, the standard stability estimate of  $u_r^n$  in  $l^\infty(L^2)$  for CN scheme in (17), the Sobolev embedding, and the Young's inequality as

$$\begin{aligned} (u_r^{n+1/2} \eta_x^{n+1/2}, \phi_r^{n+1/2})_{L^2} &\leq \|u_r^{n+1/2}\|_{L^2} \|\eta_x^{n+1/2}\|_{L^2} \|\phi_r^{n+1/2}\|_{L^\infty} \\ &\leq C \|\eta_x^{n+1/2}\|_{L^2}^2 + C_1 \|(\phi_r)_x^{n+1/2}\|_{L^2}^2. \end{aligned} \quad (24)$$

Finally, for the last nonlinear term in (21), we use the Hölder's inequality, the stability estimate of  $u_r^n$  in (17), the Agmon's inequality (eq. after (45) in [25]):

$$\|\varphi\|_{L^\infty} \leq C \|\varphi\|_{L^2}^{1/2} \|\varphi_x\|_{L^2}^{1/2}, \quad \forall \varphi \in H_0^1,$$

and the Young's inequality ( $p = 4, q = 4/3$ ), then we get

$$\begin{aligned} (u_r^{n+1/2} (\phi_r)_x^{n+1/2}, \phi_r^{n+1/2})_{L^2} &\leq \|u_r^{n+1/2}\|_{L^2} \|(\phi_r)_x^{n+1/2}\|_{L^2} \|\phi_r^{n+1/2}\|_{L^\infty} \\ &\leq C \|\phi_r^{n+1/2}\|_{L^2}^{1/2} \|(\phi_r)_x^{n+1/2}\|_{L^2}^{3/2} \\ &\leq C \|\phi_r^{n+1/2}\|_{L^2}^2 + C_2 \|(\phi_r)_x^{n+1/2}\|_{L^2}^2. \end{aligned} \quad (25)$$

To bound the consistency error (11), we use the Taylor's theorem, the Young's inequality, and the property  $(a + b + c)^2 \leq 3(a^2 + b^2 + c^2)$  for  $I_{n,1}(u)$  in (13), then we have

$$\begin{aligned} \tau_n(\phi_r^{n+1/2}) &\leq \Delta t^{3/2} I_{n,1}(u) \|\phi_r^{n+1/2}\|_{L^2} \\ &\leq \frac{3}{4} \Delta t^3 I_n(u) + \|\phi_r^{n+1/2}\|_{L^2}^2. \end{aligned} \quad (26)$$

Now, we choose coefficient  $C_1 = C_2 = \nu/4$ , and insert all bounds (20)-(26) into (19), then

$$\begin{aligned} \frac{1}{2\Delta t} \left( \|\phi_r^{n+1}\|_{L^2}^2 - \|\phi_r^n\|_{L^2}^2 \right) + \frac{\nu}{2} \|(\phi_r)_x^{n+1/2}\|_{L^2}^2 &\leq C \left[ \|\phi_r^{n+1/2}\|_{L^2}^2 + \|\partial \eta^{n+1}\|_{L^2}^2 \right. \\ &\quad \left. + \|\eta^{n+1/2}\|_{L^2}^2 + \|\eta_x^{n+1/2}\|_{L^2}^2 + \Delta t^3 I_n(u) \right]. \end{aligned} \quad (27)$$

To derive a valid error bound from (27), there should be a relation between the time step  $\Delta t$  and the viscosity coefficient  $\nu$  that is explained in the following lemma.

**Lemma 4.1.** *Let  $\Delta t < \frac{4C\nu^3}{27}$ , then it holds*

$$\begin{aligned} (1 - C\Delta t) \|\phi_r^{n+1}\|_{L^2}^2 + \nu \Delta t \|(\phi_r)_x^{n+1/2}\|_{L^2}^2 &\leq (1 + C\Delta t) \|\phi_r^n\|_{L^2}^2 + C\Delta t \left[ \|\partial \eta^{n+1}\|_{L^2}^2 \right. \\ &\quad \left. + \|\eta^{n+1/2}\|_{L^2}^2 + \|\eta_x^{n+1/2}\|_{L^2}^2 + \Delta t^3 I_n(u) \right]. \end{aligned} \quad (28)$$

*Proof.* First, rebounding the term  $\|\phi_r^{n+1/2}\|_{L^2}^2$  yields  $\frac{1}{2} \left( \|\phi_r^{n+1}\|_{L^2}^2 + \|\phi_r^n\|_{L^2}^2 \right)$  in (27). Then, if one correctly computes the constant coefficients in (20)-(26), the generic constant  $C$  in (27) will be

$$C := \max \left\{ \frac{1}{4}, \frac{\|u_x^{n+1/2}\|_{L^\infty}^2}{4}, \frac{\|u_x^{n+1/2}\|_{L^\infty}}{2}, \frac{\|u_r^{n+1/2}\|_{L^2}^2}{\nu}, \frac{27 \|u_r^{n+1/2}\|_{L^2}^4}{8\nu^3}, \frac{3}{4}, \frac{3}{2} \right\}. \quad (29)$$

From (17), one knows that the term  $\|u_r^{n+1/2}\|$  is bounded. With out loss of generality, in this paper, we assume that  $\frac{27 \|u_r^{n+1/2}\|_{L^2}^4}{8\nu^3}$  dominates the terms in (29). Finally, multiplying the resulting equation with  $2\Delta t$ , one obtains (28) with the constraint  $\Delta t < \frac{4C\nu^3}{27}$ , where  $C = (\|u_r^{n+1/2}\|_{L^2})^{-4}$ .  $\square$

**Remark 4.2.** One can bound the term  $\|(\phi_r)_x^{n+1/2}\|_{L^2}^2$  in (24)-(25) by using FE inverse estimate as (see Appendix of [37])

**Lemma 4.3.** For any  $\phi_r^{n+1} \in X^h$ , which is the FE space contains  $X^r$ , then following the inverse finite element estimate holds:

$$\|(\phi_r^{n+1})_x\|_{L^2} \leq C h^{-1/2} \|\phi_r^{n+1}\|_{L^2}. \quad (30)$$

However, by using the FE inverse estimate to bound the term  $\|(\phi_r)_x^{n+1/2}\|_{L^2}^2$  in (24)-(25), the generic constant  $C$  in (28) depends on the space discretization  $h$ , and we eventually loose  $\sqrt{h}$  convergence order.

Furthermore, the bound in (28) obtained by using the Galerkin method leads to a restriction on the time step  $\Delta t$  (see Lemma 4.1). Using stabilized methods would allow relaxing this restriction. In this paper, our concern is analyzing the error estimates optimality with respect to the different POD setting strategies, so we will consider moderate values of  $\nu$ .

**Remark 4.4.** In this paper, we construct the POD basis by using the snapshots, which are the FE solutions; thus,  $\eta^n$  bounds in Lemma 2.1 and Theorem 2.2 should be expressed in terms of the FE solution data. Now, we decompose and rebound  $\eta^n$  in (27) by taking the FE solution  $u_h^n$  into account as

$$\frac{1}{N+1} \sum_{n=0}^N \|u^n - R_r u^n\|_W^2 \leq C (h^{2l} + \Delta t^4) + \frac{1}{N+1} \sum_{n=0}^N \|u_h^n - R_r u_h^n\|_W^2 \quad (31a)$$

$$\frac{1}{N+1} \sum_{n=0}^{N+1} \|\partial(u^n - R_r u^n)\|_{L^2}^2 \leq C (h^{2l+1} + \Delta t^3) + \frac{1}{N+1} \sum_{n=0}^N \|\partial(u_h^n - R_r u_h^n)\|_{L^2}^2, \quad (31b)$$

where  $l$  is the FE interpolation order.

*Proof.* We start proving with  $W = H_0^1$  in (31a). By using the definition of the Ritz projection (16), we have

$$\begin{aligned} \|\nabla(u^n - R_r u^n)\|_{L^2}^2 &= (\nabla(u^n - R_r u^n), \nabla(u^n - R_r u^n)), \\ &= (\nabla(u^n - R_r u^n), \nabla(u^n - R_r u_h^n)), \\ &\leq \|\nabla(u^n - R_r u^n)\|_{L^2} \|\nabla(u^n - R_r u_h^n)\|_{L^2}. \end{aligned} \quad (32)$$

Then, by adding and subtracting the FE solution  $u_h^n$  in (32) and summing the resulting inequality from  $n = 0$  to  $N$  give

$$\begin{aligned} \|\nabla(u^n - R_r u^n)\|_{L^2}^2 &\leq \|\nabla(u^n - u_h^n)\|_{L^2}^2 + \|\nabla(u_h^n - R_r u_h^n)\|_{L^2}^2, \\ \frac{1}{N+1} \sum_{n=0}^N \|\nabla(u^n - R_r u^n)\|_{L^2}^2 &\leq C (h^{2l} + \Delta t^4) + \frac{1}{N+1} \sum_{n=0}^N \|\nabla(u_h^n - R_r u_h^n)\|_{L^2}^2. \end{aligned} \quad (33)$$

For  $W = L^2$  case, we still revisit the definition of the Ritz projection (16) and choose  $v_r = R_r u$ , then we have

$$\|\nabla R_r u\|_{L^2} \leq \|\nabla u\|_{L^2}. \quad (34)$$

Then, by adding and subtracting the FE solution,  $u_h^n$  in  $\|u^n - R_r u^n\|_{L^2}$ , applying to the Poincaré inequality, the relation in (34), and summing from  $n = 0$  to  $N$  give

$$\begin{aligned} \|u^n - R_r u^n\|_{L^2}^2 &\leq \|u^n - u_h^n\|_{L^2}^2 + \|R_r(u^n - u_h^n)\|_{L^2}^2 + \|u_h^n - R u_h^n\|_{L^2}^2, \\ &\leq \|u^n - u_h^n\|_{L^2}^2 + C_p \|\nabla R_r(u^n - u_h^n)\|_{L^2}^2 + \|u_h^n - R u_h^n\|_{L^2}^2, \\ \frac{1}{N+1} \sum_{n=0}^N \|u^n - R_r u^n\|_{L^2}^2 &\leq C(h^{2l} + \Delta t^4) + \frac{1}{N+1} \sum_{n=0}^N \|u_h^n - R u_h^n\|_{L^2}^2. \end{aligned} \quad (35)$$

Finally, to rebound the term  $\|\partial(u^n - R_r u^n)\|$ , we follow the similar steps in (35) and get the following:

$$\frac{1}{N+1} \sum_{n=0}^N \|\partial(u^n - R_r u^n)\|_{L^2}^2 \leq C(h^{2l+1} + \Delta t^3) + \frac{1}{N+1} \sum_{n=0}^N \|\partial(u_h^n - R u_h^n)\|_{L^2}^2. \quad (36)$$

Thus, overall all the squares of the POD projection errors are bounded with  $h^2$  (we are using the linear FEs, i.e.,  $l = 1$ ) and  $\Delta t^3$  in space and time, respectively. In our numerical setting, we choose  $h \approx 2\Delta t$ ; thus, in short, it is bounded with  $\Delta t^2$ .  $\square$

Now, in the following two sections, by using Lemma 4.1, we continue to derive and discuss DQ CN-POD-ROM errors in different norms considering  $L^2(\Omega)$  and  $H_0^1(\Omega)$  POD bases that will lead to different consistency error estimates.

**Remark 4.5.** *For the construction of all methods, Crank-Nicolson and Galerkin discretizations are common; thus, when we label the name of the models, we drop CN and POD acronyms. For example, from now on, when we refer to the DQ CN-POD-ROM with  $L^2(\Omega)$  basis, we use the DQ-L2 acronym.*

#### 4.1 The $l^\infty(L^2)$ Error Estimates

In this section, we provide the  $l^\infty(L^2)$  error estimates for the DQ-ROM (9), considering both  $L^2(\Omega)$  and  $H_0^1(\Omega)$  POD spaces. Specifically, we discuss the optimality behavior of the  $l^\infty(L^2)$  DQ-L2 and DQ-H01 error in the following Theorem 4.6 and Theorem 4.8, respectively.

**Theorem 4.6.** *Assume that  $\Delta t \leq \frac{2C\nu^3}{27}$ , then the  $l^\infty(L^2)$  DQ-L2 error is bounded by*

$$\begin{aligned} \max_{0 \leq k \leq N} \|e^k\|_{L^2}^2 &\leq C \left[ \|\phi_r^0\|_{L^2}^2 + \sum_{i=r+1}^d \lambda_i^{\text{DQ}} \left( \|\varphi_i - R_r \varphi_i\|_{L^2}^2 + \|(\varphi_i - R_r \varphi_i)_x\|_{L^2}^2 \right) \right. \\ &\quad \left. + \Delta t^2 + \Delta t^4 I(u) \right]. \end{aligned} \quad (37)$$

*Proof.* To apply the discrete Gronwall's lemma to Lemma 4.1, we first consider the following notations:

$$\begin{aligned} \alpha_n &:= \|\phi_r^n\|_{L^2}^2 \geq 0, \\ \beta_n &:= C\Delta t \left( \|\partial\eta^{n+1}\|_{L^2}^2 + \|\eta^{n+1/2}\|_{L^2}^2 + \|\eta_x^{n+1/2}\|_{L^2}^2 + \Delta t + \Delta t^3 I_n(u) \right) \geq 0, \\ C &= \frac{27}{4C\nu^3} \geq 0 \quad \text{from Lemma 4.1.} \end{aligned} \quad (38)$$

By using notations in (38), we rewrite (28) as follows:

$$(1 - C\Delta t)\alpha_{n+1} \leq (1 + C\Delta t)\alpha_n + \beta_n \quad \forall n = 0, \dots, N-1. \quad (39)$$

By using the discrete Gronwall's lemma (see Lemma 10.4 in [37]) in (39), and if the small time step assumption, i.e.,  $\Delta t \leq 0.5 C^{-1} = \frac{2C\nu^3}{27}$ , is guaranteed, then the following inequality holds:

$$\begin{aligned} \max_{k=0,\dots,N} \|\phi_r^k\|_{L^2}^2 &\leq e^{4CT} \|\phi_r^0\|_{L^2}^2 \\ &+ 2Ce^{4CT} \sum_{n=0}^{N-1} \Delta t \left( \|\partial\eta^{n+1}\|_{L^2}^2 + \|\eta^{n+1}\|_{L^2}^2 + \|\eta_x^{n+1}\|_{L^2}^2 + \Delta t + \Delta t^3 I_n(u) \right). \end{aligned} \quad (40)$$

Now, add  $\|\eta^k\|_{L^2}^2$  to both sides of (40) to obtain

$$\begin{aligned} \max_{0 \leq k \leq N} \|e^k\|_{L^2}^2 &\leq \max_{0 \leq k \leq N} \|\eta^k\|_{L^2}^2 + Ce^{4CT} \left[ \|\phi_r^0\|_{L^2}^2 + \Delta t^2 + \Delta t^4 I(u) \right. \\ &\left. + \sum_{n=0}^{N-1} \Delta t \left( \|\partial\eta^{n+1}\|_{L^2}^2 + \|\eta^{n+1}\|_{L^2}^2 + \|\eta_x^{n+1}\|_{L^2}^2 \right) \right]. \end{aligned} \quad (41)$$

Using  $2(N+1)\Delta t = 2T + \Delta t \leq 3T$  relation and updating the generic constant  $C$  in (41) give

$$\begin{aligned} \max_{0 \leq k \leq N} \|e^k\|_{L^2}^2 &\leq C \left[ \max_{0 \leq k \leq N} \|\eta^k\|_{L^2}^2 + \|\phi_r^0\|_{L^2}^2 + \Delta t^2 + \Delta t^4 I(u) \right. \\ &\left. + \frac{1}{2N+1} \sum_{n=0}^{N-1} \left( \|\partial\eta^{n+1}\|_{L^2}^2 + \|\eta^{n+1}\|_{L^2}^2 + \|\eta_x^{n+1}\|_{L^2}^2 \right) \right]. \end{aligned} \quad (42)$$

Now, use (6b) in Lemma 2.1 and (7c) in Theorem 2.2 with  $W = L^2$  and  $H_0^1$ . This ends the proof.  $\square$

Now, we discuss the optimality behavior of the  $l^\infty(L^2)$  DQ-L2 error. Since the second term on the right-hand side of (37) is bounded by the  $H_0^1$  norm, the  $l^\infty(L^2)$  DQ-L2 error bound yields a suboptimal error estimate with respect to the ROM discretization.

Before presenting the  $l^\infty(L^2)$  DQ-H01 error, we provide some bounds related to the Ritz projection when considering the  $H_0^1(\Omega)$  POD space framework, which will be used in Theorem 4.8.

**Lemma 4.7.** *(Bounds for Ritz Projection) The Ritz projection satisfies the following bounds if  $H_0^1(\Omega)$  POD basis is used:*

$$\begin{cases} \|\varphi_i - R_r \varphi_i\|_{L^2} = \|\varphi_i\|_{L^2} \\ \|(\varphi_i - R_r \varphi_i)_x\|_{L^2} = 1, \quad \forall i = r+1, \dots, d. \end{cases} \quad (43)$$

*Proof.* One can expand the term  $R_r \varphi_i \in X^r$  by the considering first  $r$  POD modes as

$$R_r \varphi_i := \sum_{j=1}^r (R_r \varphi_i, \varphi_j)_{H_0^1} \varphi_j \quad (44)$$

Let  $W$  denote either  $L^2$  or  $H_0^1$ . Then, by using (44), we get the following:

$$\begin{aligned}
\|\varphi_i - R_r \varphi_i\|_W^2 &= \left( \varphi_i - \sum_{j=1}^r (R_r \varphi_i, \varphi_j)_{H_0^1} \varphi_j, \varphi_i - \sum_{k=1}^r (R_r \varphi_i, \varphi_k)_{H_0^1} \varphi_k \right)_W \\
&= \|\varphi_i\|_W^2 - \sum_{j=1}^r (R_r \varphi_i, \varphi_j)_{H_0^1} (\varphi_j, \varphi_i)_W - \sum_{k=1}^r (R_r \varphi_i, \varphi_k)_{H_0^1} (\varphi_k, \varphi_i)_W \\
&\quad + \sum_{j,k=1}^r (R_r \varphi_i, \varphi_j)_{H_0^1} (R_r \varphi_i, \varphi_k)_{H_0^1} (\varphi_j, \varphi_k)_W \\
&= \|\varphi_i\|_W^2 - \sum_{j=1}^r (\varphi_i, \varphi_j)_{H_0^1} (\varphi_j, \varphi_i)_W - \sum_{k=1}^r (\varphi_i, \varphi_k)_{H_0^1} (\varphi_k, \varphi_i)_W \\
&\quad + \sum_{j,k=1}^r (\varphi_i, \varphi_j)_{H_0^1} (\varphi_i, \varphi_k)_{H_0^1} (\varphi_j, \varphi_k)_W \\
&= \|\varphi_i\|_W^2
\end{aligned} \tag{45}$$

where  $(\varphi_i, \varphi_k)_{H_0^1} = 0$ ,  $\forall i = r+1, \dots, d$ ,  $j, k = 1, \dots, r$ . If  $W = L^2$ , then  $\|\varphi_i\|_W^2 = \|\varphi_i\|_{L^2}^2$  will keep the same; otherwise,  $W = H_0^1$ , then  $\|\varphi_i\|_{H_0^1}^2 = 1$ . This ends the proof.  $\square$

**Theorem 4.8.** Assume that  $\Delta t \leq \frac{2\mathcal{C}\nu^3}{27}$ , then the  $l^\infty(L^2)$  DQ-H01 error is bounded by

$$\max_{0 \leq k \leq N} \|e^k\|_{L^2}^2 \leq C \left[ \|\phi_r^0\|_{L^2}^2 + \sum_{i=r+1}^d \lambda_i^{\text{DQ}} (1 + \|\varphi_i\|_{L^2}^2) + \Delta t^2 + \Delta t^4 I(u) \right]. \tag{46}$$

*Proof.* The derivation of the  $l^\infty(L^2)$  DQ-H01 error bound is exactly the same as the error bound for the  $l^\infty(L^2)$  DQ-L2 error bound (37). Now, we consider the  $H_0^1(\Omega)$  POD basis; thus, we need to rebound the right-hand side of (37) by using the properties in (43) in Lemma 4.7. This ends the proof.  $\square$

Now, we discuss the optimality behavior of the  $l^\infty(L^2)$  DQ-H01 error bound. One can observe that the  $l^\infty(L^2)$  DQ-H01 error (46) has optimal behavior. Furthermore, in Definition 4.9, we discuss several types of optimality: *truly optimal* and *optimal-I* have been addressed in [19], and *optimal-II*, which is new and discussed at Definition 4.6 in [23].

**Definition 4.9.** Let  $X^r \subset \mathcal{H}$  be the span of the first  $r$  POD modes, and assume  $X^r$  is also contained in  $W$ . Let  $P_r : \mathcal{H} \rightarrow \mathcal{H}$  be the orthogonal POD projection onto  $X^r$ , and let  $\Pi_r^W : W \rightarrow W$  be the  $W$ -orthogonal projection onto  $X^r$ . Also, let  $s$  be the number of positive POD eigenvalues. Then, the ROM discretization error is

$$\text{truly optimal: if a ROM discretization error} \leq C \left( \max_{1 \leq k \leq N} \|u^k - \Pi_r^W u^k\|_W^2 \right), \tag{47a}$$

$$\text{optimal-I: if a ROM discretization error} \leq C \left( \sum_{i=r+1}^s \lambda_i \|\varphi_i\|_W^2 \right), \tag{47b}$$

$$\text{optimal-II: if a ROM discretization error} \leq C \left( \sum_{i=r+1}^s \lambda_i \|\varphi_i - \Pi_r^W \varphi_i\|_W^2 \right), \tag{47c}$$

where the constant  $C$  above should be independent of all discretization parameters but may depend on the solution data and the problem data.

Among these optimality types, we conclude that (46) has optimal-I behavior with respect to the ROM discretization.

## 4.2 The Natural-Norm Error Estimates

In this section, we provide the natural-norm, i.e.,  $(l^\infty(L^2) \cap l^2(H_0^1))$  error estimates for the DQ-ROM (9) considering both  $L^2(\Omega)$  and  $H_0^1(\Omega)$  POD spaces. Specifically, we discuss the optimality behavior of the natural-norm DQ-L2 and DQ-H01 error in the following Theorem 4.10 and Theorem 4.11, respectively.

**Theorem 4.10.** *The natural-norm DQ-L2 error is bounded by*

$$\max_{0 \leq k \leq N} \|e^k\|_{L^2}^2 + \nu \Delta t \sum_{n=0}^{N-1} \|e_x^{n+1/2}\|_{L^2}^2 \leq C \left[ \|\phi_r^0\|_{L^2}^2 + \sum_{i=r+1}^d \lambda_i^{\text{DQ}} \left( \|\varphi_i - R_r \varphi_i\|_{L^2}^2 + \|(\varphi_i - R_r \varphi_i)_x\|_{L^2}^2 \right) + \Delta t^2 + \Delta t^4 I(u) \right]. \quad (48)$$

*Proof.* We start derivation with rearranging (27) as follows:

$$\begin{aligned} (\|\phi_r^{n+1}\|_{L^2}^2 - \|\phi_r^n\|_{L^2}^2) + \nu \Delta t \|(\phi_r)_x^{n+1/2}\|_{L^2}^2 &\leq C \Delta t \left[ \|\phi_r^{n+1}\|_{L^2}^2 + \|\phi_r^n\|_{L^2}^2 \right. \\ &\quad \left. + \|\partial \eta^{n+1}\|_{L^2}^2 + \|\eta^{n+1/2}\|_{L^2}^2 + \|\eta_x^{n+1/2}\|_{L^2}^2 + \Delta t + \Delta t^3 I_n(u) \right], \end{aligned} \quad (49)$$

where  $C = \frac{27}{4C\nu^3}$ . The first two terms on the right-hand side of (49) are in ROM space; thus, they are bounded thanks to the standard stability estimate for the ROM solution. Furthermore, the common coefficient of the right-hand side of (49), i.e.,  $C\Delta t$  is also well balanced. Then, adding  $\|\eta^k\|_{L^2}^2$  and  $\nu \Delta t \sum_{n=0}^{N-1} \|\eta_x^{n+1/2}\|_{L^2}^2$  terms to both sides of (49) after summing from  $n = 0$  to  $n = N - 1$  gives

$$\begin{aligned} \max_{0 \leq k \leq N} \|e^k\|_{L^2}^2 + \nu \Delta t \sum_{n=0}^{N-1} \|e_x^{n+1/2}\|_{L^2}^2 &\leq C \left[ \max_{0 \leq k \leq N} \|\eta^k\|_{L^2}^2 + \|\phi_r^0\|_{L^2}^2 \right. \\ &\quad \left. + \Delta t \sum_{n=0}^{N-1} \left( \|\partial \eta^{n+1}\|_{L^2}^2 + \|\eta^{n+1/2}\|_{L^2}^2 + \|\eta_x^{n+1/2}\|_{L^2}^2 \right) + \Delta t^2 + \Delta t^4 I(u) \right], \end{aligned} \quad (50)$$

Use  $2(N + 1)\Delta t = 2T + \Delta t \leq 3T$  relation and update the generic constant  $C$  in (50), then apply (6b) in Lemma 2.1 and (7c) in Theorem 2.2 with  $W = L^2$  and  $H_0^1$ . This ends proof.  $\square$

**Theorem 4.11.** *The natural-norm DQ-H01 error is bounded by*

$$\begin{aligned} \max_{0 \leq k \leq N} \|e^k\|_{L^2}^2 + \nu \Delta t \sum_{n=0}^{N-1} \|e_x^{n+1/2}\|_{L^2}^2 &\leq C \left[ \|\phi_r^0\|_{L^2}^2 + \sum_{i=r+1}^d \lambda_i^{\text{DQ}} (1 + \|\varphi_i\|_{L^2}^2) \right. \\ &\quad \left. + \Delta t^2 + \Delta t^4 I(u) \right]. \end{aligned} \quad (51)$$

*Proof.* The derivation of the natural-norm DQ-H01 error bound is exactly the same as the error bound for the natural-norm DQ-L2 error bound (48). Now, we consider the  $H_0^1(\Omega)$  POD basis; thus, we need to rebound the right-hand side of (48) by using the properties in (43) in Lemma 4.7. This ends the proof.  $\square$

**Remark 4.12.** *We briefly provide the  $l^\infty(L^2)$  and natural-norm noDQ-L2 and noDQ-H01 error estimates. To obtain the  $l^\infty(L^2)$  and natural-norm noDQ error bounds, one can proceed similarly to the above proof using the  $L^2$  projection instead of the Ritz projection. The  $l^\infty(L^2)$  and natural-norm error bounds are the same. Specifically, the  $l^\infty(L^2)$  and*

natural-norm noDQ-L2 error bound is provided in (52a), and the noDQ-H01 error bound is provided in (52b).

$$\mathcal{E} \leq C \left[ \|\phi_r^0\|_{L^2}^2 + \sum_{i=r+1}^d \lambda_i^{\text{noDQ}} \left( \|\varphi_i\|_{L^2}^2 + \|(\varphi_i)_x\|_{L^2}^2 \right) + \Delta t^2 + \Delta t^4 I(u) \right], \quad (52a)$$

$$\mathcal{E} \leq C \left[ \|\phi_r^0\|_{L^2}^2 + \sum_{i=r+1}^d \lambda_i^{\text{noDQ}} (1 + \|\varphi_i\|_{L^2}^2) + \Delta t^2 + \Delta t^4 I(u) \right]. \quad (52b)$$

Based on the noDQ error bounds (52a)-(52b), the  $l^\infty(L^2)$  and natural-norm noDQ and DQ ROM errors have the same optimal behavior.

## 5 Numerical Results

In this section, we provide numerical results for the Burgers equation (1) with the following initial condition

$$u_0(x) = \begin{cases} 1, & x \in (0, 1/2], \\ 0, & x \in (1/2, 1]. \end{cases} \quad (53)$$

This condition generates a smooth solution at any  $t > 0$ , with an infinite time gradient at  $t = 0$ . This allows us to test the role of the difference quotients. To obtain a full order model (FOM) data, we solve (1) by using the finite element method considering  $\nu = 10^{-2}$ ,  $f = 0$ , mesh size  $h = 1/512$ , piecewise linear finite element spatial discretization, and Crank-Nicolson time discretization. A very small time step, i.e.,  $\Delta t = 10^{-3}$ , is taken to obtain the errors due to the POD discretization.

For all test cases, we compute two different absolute norm ROM errors and the Ritz projection error:

$$\mathcal{E}_{l^\infty(L^2)} = \max_{0 \leq k \leq N} \|e^k\|_{L^2}^2, \quad (54a)$$

$$\mathcal{E}_{l^\infty(L^2) \cap l^2(H_0^1)} = \max_{0 \leq k \leq N} \|e^k\|_{L^2}^2 + \nu \Delta t \sum_{n=0}^{N-1} \|e_x^{n+1/2}\|_{L^2}^2, \quad (54b)$$

$$\eta_{l^\infty(L^2)} = \max_{0 \leq k \leq N} \|u^k - R_r u^k\|_{L^2}^2. \quad (54c)$$

### 5.0.1 noDQ CN-POD-ROM Results

In this section, we numerically discuss the optimality behavior of the  $l^\infty(L^2)$  and natural-norm noDQ-L2 and noDQ-H01 methods. Based on the noDQ error estimates in (52a)-(52b) in Remark 4.12, we define the following RHS terms:

$$\text{noDQ-RHS1} = \sum_{i=r+1}^d \lambda_i^{\text{noDQ}} \left( \|\varphi_i\|_{L^2}^2 + \|(\varphi_i)_x\|_{L^2}^2 \right) + \Delta t^2 + \Delta t^4 I(u), \quad (55a)$$

$$\text{noDQ-RHS2} = \sum_{i=r+1}^d \lambda_i^{\text{noDQ}} \|\varphi_i\|_{L^2}^2 + \Delta t^2 + \Delta t^4 I(u). \quad (55b)$$

In the top left plot of Figure 1, considering the  $L^2(\Omega)$  POD basis, we plot the noDQ-RHS1, noDQ-RHS2 defined in (55a)-(55b) and  $l^\infty(L^2)$ , natural-norm noDQ-L2 errors defined in (54a)-(54b), and the Ritz projection error (54c). We observe that the  $l^\infty(L^2)$

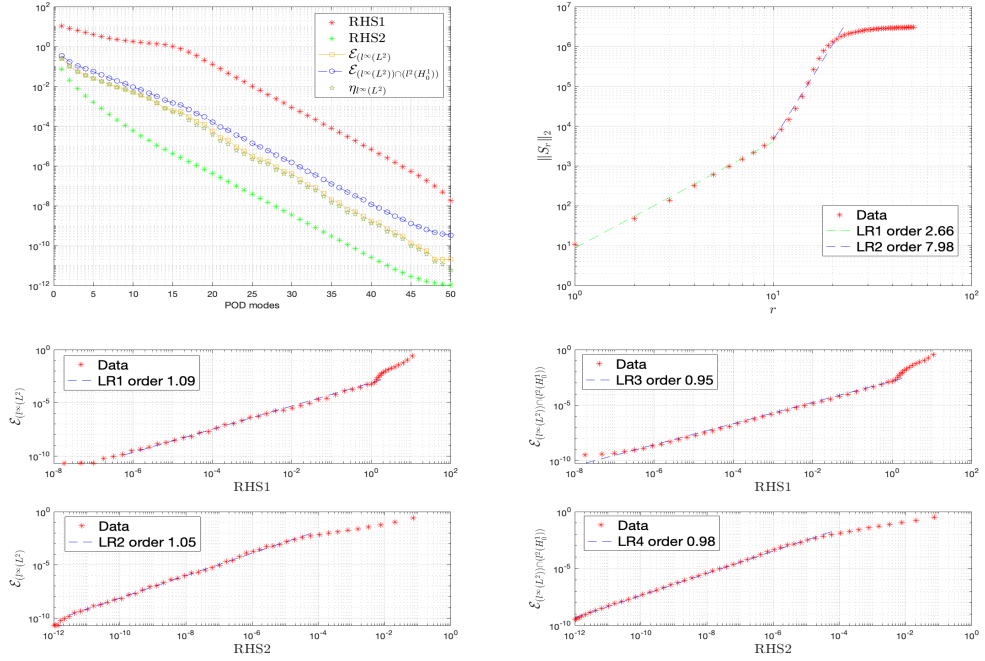


**Figure 1:** Optimality behavior of the  $l^\infty(L^2)$  and natural-norm noDQ-L2 errors.

and natural-norm noDQ-L2 errors stay between the RHS1 and RHS2, and both RHS terms have similar behavior with the errors. The top right plot shows how the gradient of the POD modes changes as  $r$  changes. For the bottom plots in Figure 1, we plot the linear regression orders for  $l^\infty(L^2)$  and natural-norm noDQ-L2 errors, from left to right, respectively.

In Figure 2, we regenerate the same errors and RHS terms for the  $H_0^1(\Omega)$  POD basis. The numerical results in Figures 1 and 2 show that all noDQ error bounds for both  $L^2(\Omega)$  and  $H_0^1(\Omega)$  POD bases are optimal. In other words, the  $L^2$  and  $H_0^1$  POD space framework yield the same results. However, we prove that the  $l^\infty(L^2)$  and natural-norm noDQ-L2 error bound 52a in Remark 4.12 is suboptimal. The possible explanation for that situation is the behavior of the  $\|S_r\|$  and  $\|M_r^{-1}\|$ . The top right plots in Figures 1 and 2 show that for certain POD modes, which are used to compute the linear regression orders,  $\|S_r\|$  and  $\|M_r^{-1}\|$  do change slightly.

Figure 3 plots the noDQ-L2 and noDQ-H01 solutions with different  $r$  values. For both  $r$  values, we observe that the noDQ-H01 yields slightly more accurate results than the noDQ-L2, especially for low  $r$  values such as  $r = 5$ .

### 5.0.2 DQ CN-POD-ROM Results

In this section, we numerically discuss the optimality behavior of the  $l^\infty(L^2)$  and natural-norm DQ ROM errors considering  $L^2(\Omega)$  and  $H_0^1(\Omega)$  POD bases. Based on the DQ-L2

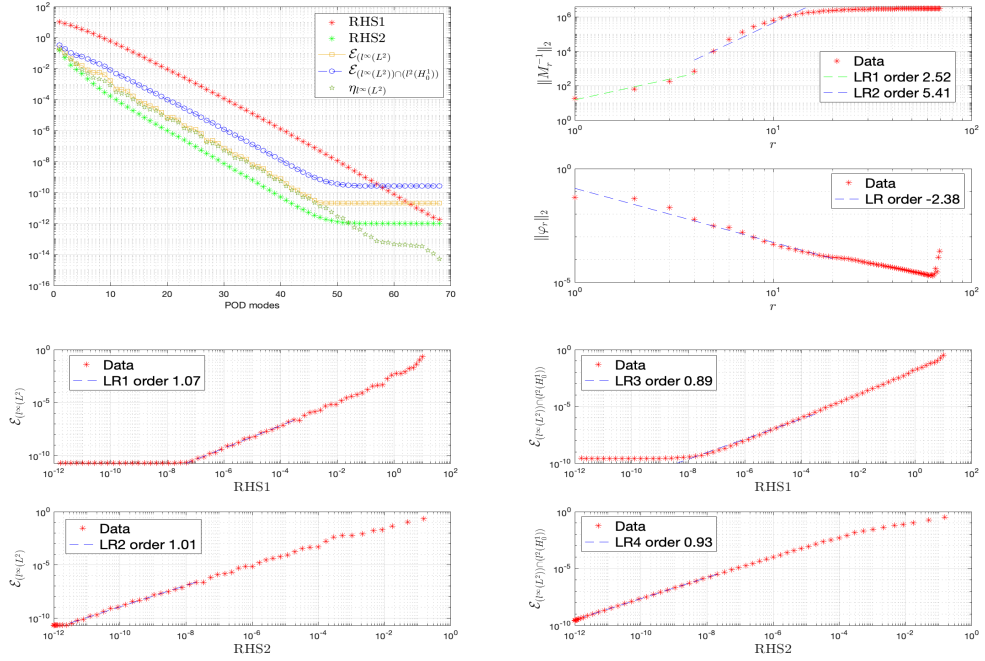


**Figure 2:** Optimality behavior of the  $l^\infty(L^2)$  and natural-norm noDQ-H01 errors.

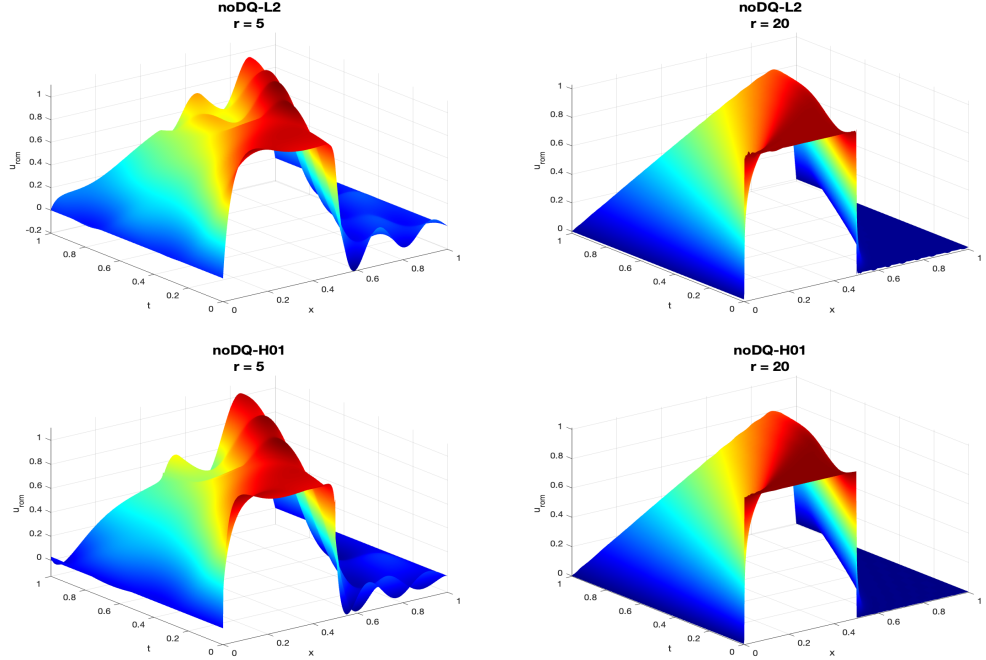


**Figure 3:** Comparison of the noDQ-L2 and noDQ-H01 solution plots with two different  $r$  values.

error estimate in (37), we define the following RHS terms:

$$\text{DQ-RHS1} = \sum_{i=r+1}^d \lambda_i^{\text{DQ}} \left( \|\varphi_i - R_r \varphi_i\|_{L^2}^2 + \|(\varphi_i - R_r \varphi_i)_x\|_{L^2}^2 \right) + \Delta t^2 + \Delta t^4 I(u), \quad (56a)$$

$$\text{DQ-RHS2} = \sum_{i=r+1}^d \lambda_i^{\text{DQ}} \|\varphi_i - R_r \varphi_i\|_{L^2}^2 + \Delta t^2 + \Delta t^4 I(u). \quad (56b)$$

to discuss their optimality behavior. In the top left plot of Figure 4, considering the  $L^2(\Omega)$  POD basis, we plot the DQ-RHS1, DQ-RHS2 defined in (56a)-(56b) and  $l^\infty(L^2)$ , natural-norm DQ-L2 errors defined in (54a)-(54b), and the Ritz projection error (54c). For the bottom plots in Figure 4, we plot the linear regression orders for  $l^\infty(L^2)$  and natural-norm DQ-L2 errors, from left to right, respectively. Based on the linear regression orders in Figure 4, we numerically observe that the  $l^\infty(L^2)$  DQ-L2 error bound is superoptimal; however, in (37), we theoretically prove that it is suboptimal.

In Figure 5, we plot the  $l^\infty(L^2)$  and natural-norm DQ-H01 errors with corresponding RHS terms, which are defined in (57a)-(57b) to discuss their optimality behavior.

$$\text{DQ-RHS3} = \sum_{i=r+1}^d \lambda_i^{\text{DQ}} (\|\varphi_i\|_{L^2}^2 + \|(\varphi_i)_x\|_{L^2}^2) + \Delta t^2 + \Delta t^4 I(u), \quad (57a)$$

$$\text{DQ-RHS4} = \sum_{i=r+1}^d \lambda_i^{\text{DQ}} \|\varphi_i\|_{L^2}^2 + \Delta t^2 + \Delta t^4 I(u). \quad (57b)$$

The top-left plot in Figure 5 shows a sudden decrease in the  $l^\infty(L^2)$  and natural-norm DQ-H01 errors arise when a large enough number of POD modes is attempted. We think this may be related to the sharp gradients of the exact solution that are well represented on the DQ ROM basis only when its dimension is large enough. Based on the linear regression orders, we numerically observe that the  $l^\infty(L^2)$  DQ-H01 error bound is superoptimal; however, in (46), we theoretically prove that it is optimal.

The numerical results in Figures 4 and 5 show that  $l^\infty(L^2)$  DQ-L2 and DQ-H01 error bounds are superoptimal, whereas natural-norm DQ-L2 and DQ-H01 error bounds are optimal. However, we theoretically prove that the  $l^\infty(L^2)$  DQ-L2 error bound 37 in Theorem 4.6 is suboptimal.

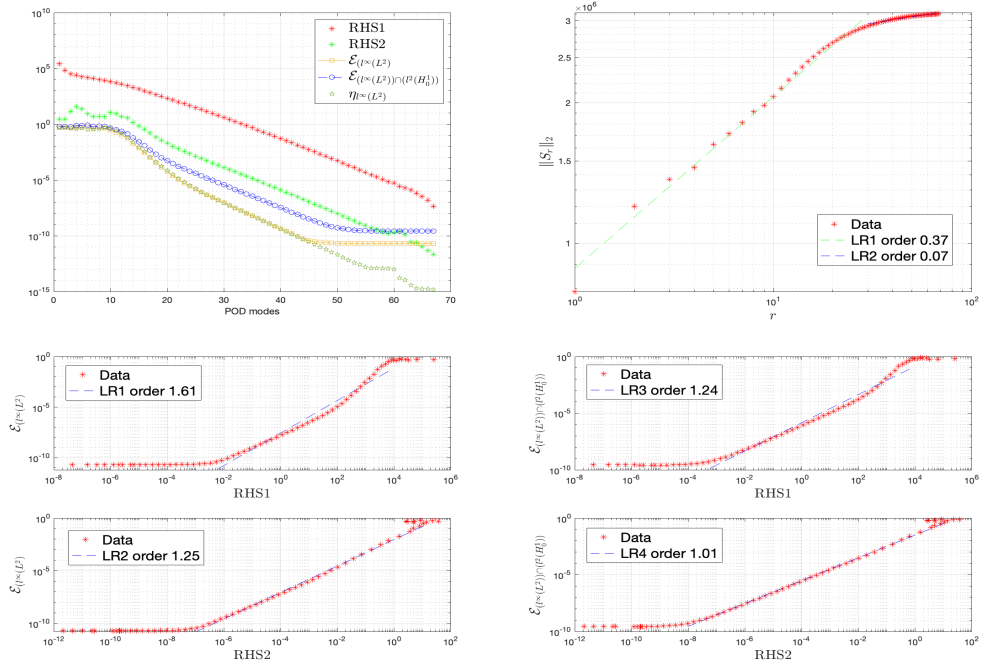


**Figure 4:** Optimality behavior of the  $l^\infty(L^2)$  and natural-norm DQ-L2 errors.

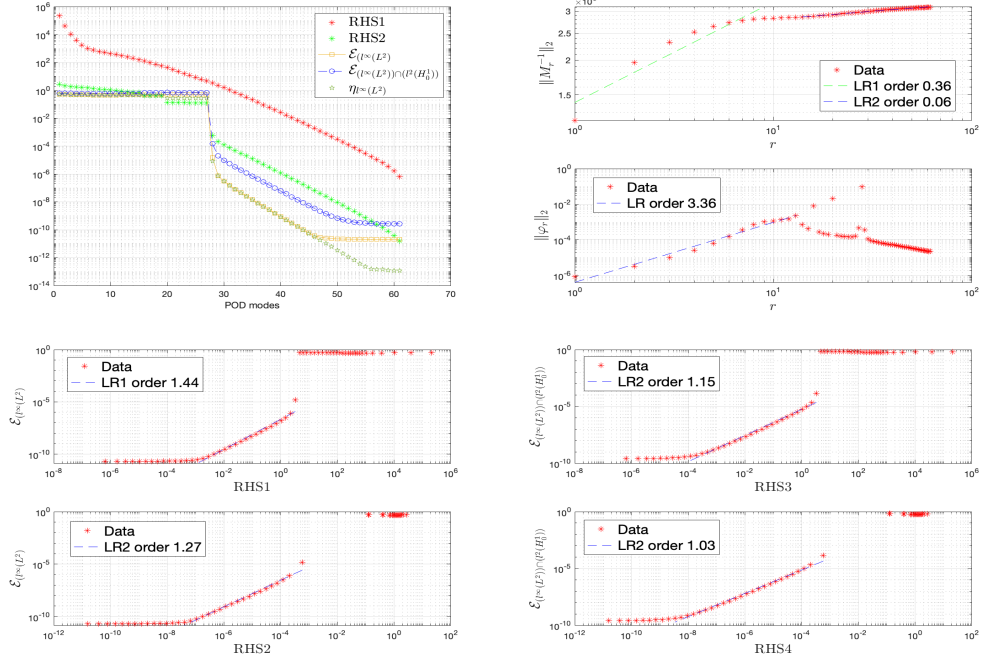


**Figure 5:** Optimality behavior of the  $l^\infty(L^2)$  and natural-norm DQ-H01 errors.

Figure 6 plots the DQ-L2 and DQ-H01 solutions with different  $r$  values. Specifically, we plot the DQ-L2 and DQ-H01 solutions for  $r = 13$  and  $r = 28$ . For  $r = 13$ , the DQ-H01 solution is less accurate than the DQ-L2 one since the ROM dimension  $r$  does not exceed the threshold value. Furthermore, the plots show that when enough POD modes are guaranteed, the DQ-H01 solution rapidly yields an accurate solution.

### 5.0.3 noDQ and DQ CN-POD-ROM Comparison

In this section, we numerically compare and discuss the noDQ and DQ ROM errors considering both POD spaces and norm errors. In the left plot of Figure 7, we plot the  $l^\infty(L^2)$  noDQ-L2, noDQ-H01, DQ-L2, and DQ-H01. Until  $r = 28$ , the noDQ-L2, noDQ-H01, and DQ-L2 errors decrease progressively, while the DQ-H01 error has a drastic decreasing behavior. After  $r = 28$ , all errors have similar behavior. However, overall there is no strict behavior between the noDQ and DQ results to compare which one has larger errors than the other.

In the right plot of Figure 7, we plot the natural-norm noDQ-L2, noDQ-H01, DQ-L2, and DQ-H01 errors. The noDQ and DQ error behaviors are more explicit in this plot than in the left one. For all  $r$  values, noDQ-L2 and noDQ-H01 errors are almost the same and lower than the DQ errors. Furthermore, as we observe in the left plot, the noDQ-L2, noDQ-H01, and DQ-L2 errors decrease progressively while the DQ-H01 error stagnates until  $r = 28$  and when it guarantees enough POD modes, it starts to gradually decrease.

Based on the bottom left plots in Figures 1-2 and Figures 4-5, it is remarkable that the regression orders of the  $l^\infty(L^2)$  noDQ-L2, noDQ-H01, DQ-L2, and DQ-H01 errors are close to 1 and 1.5, respectively. This could be due to the taking into account the time dependency by the DQs inner products.

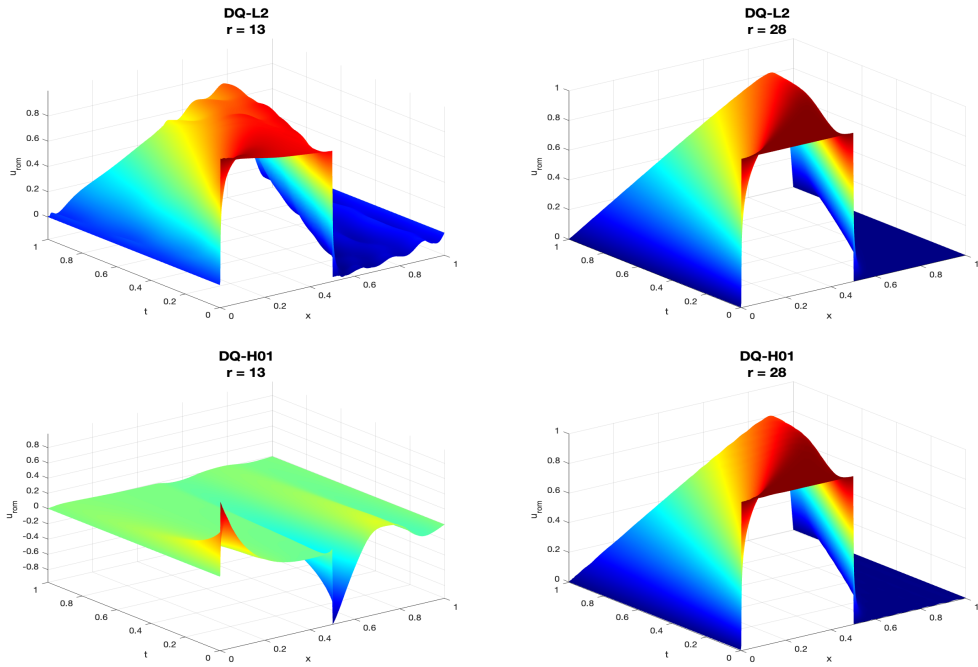


**Figure 6:** Comparison of the DQ-L2 and DQ-H01 solution plots with two different  $r$  values.

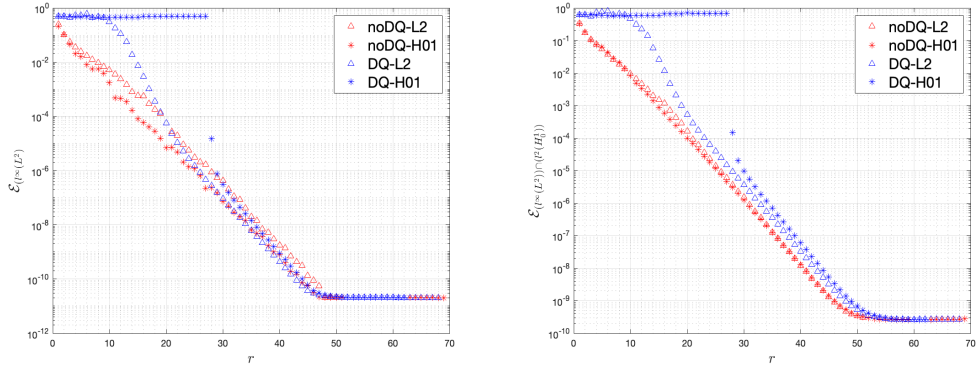


**Figure 7:**  $l^\infty(L^2)$  (left) and natural-norm (right) POD-ROM errors with  $L^2(\Omega)$  and  $H_0^1(\Omega)$  POD bases with varied  $r$  values.

## 6 Conclusions

In this paper, we provided uniform ROM error bounds of nonlinear PDEs, considering the Burgers equation as the first preliminary step considering the DQs. Overall, we theoretically proved and numerically investigated the optimality behavior of the DQ ROM error bounds by considering  $L^2(\Omega)$  and  $H_0^1(\Omega)$  spaces. Furthermore, we provided the noDQ ROM errors without any theoretical support to make a clear and complete conclusion.

The main results of this paper can be summarized as follows: (i) At the theoretical level, we derived four different DQ ROM error bounds by considering two error norms, i.e.,  $l^\infty(L^2)$  and natural-norm, and two different POD space frameworks, i.e.,  $L^2(\Omega)$  and  $H_0^1(\Omega)$  POD spaces. (ii) In Section 4.1, we theoretically proved that the  $l^\infty(L^2)$  DQ-L2 error is

suboptimal whereas  $l^\infty(L^2)$  DQ-H01 error is optimal with respect to the ROM discretization. (iii) In Section 4.2, we obtained the same theoretical results obtained in Section 4.1 for the natural-norm DQ-L2 and DQ-H01 errors. (iv) In Section 5, we illustrated numerical results calculated for the Burgers equation (1) with an initial condition (53) and numerically discussed the optimality behavior of the DQ ROM errors.

In Section 5, we numerically showed that the  $l^\infty(L^2)$  and natural-norm DQ-L2 errors are superoptimal and optimal, respectively, whereas the theoretical error bounds 37 and 48 conclude that they are suboptimal. Furthermore, numerical results illustrated that  $l^\infty(L^2)$  and natural-norm DQ-H01 errors are superoptimal and optimal, respectively. However, the theoretical and numerical results do not match only for the  $l^\infty(L^2)$  DQ-H01 case since we theoretically proved that the  $l^\infty(L^2)$  DQ-H01 error bound 46 is optimal.

Moreover, to provide a clear explanation for why the  $l^\infty(L^2)$  DQ-L2 and DQ-H01 errors have numerically superoptimality behavior, whereas the noDQ-L2 and noDQ-H01 errors have numerically optimal behavior, we compared the  $l^\infty(L^2)$  noDQ-L2, noDQ-H01, DQ-L2, and DQ-H01 errors. We believe that considering the time dependency by the DQ inner products increases the linear regression orders.

Finally, we compared the noDQ-L2 with noDQ-H01 and DQ-L2 with DQ-H01 solution plots to understand how the POD space framework affects the accuracy of the solution for both noDQ and DQ cases. For the noDQ case, we concluded that noDQ-L2 and noDQ-H01 yield similar results; however, for a low  $r$  value, the noDQ-H01 solution is slightly more accurate than the noDQ-L2. However, the comparison between the DQ-L2 and DQ-H01 is quite different than the noDQ one. Specifically, we observed that the DQ-H01 yields an accurate solution after enough POD modes are guaranteed but reaching the accurate results is quicker than the DQ-L2.

Extending and improving the effectiveness of the DQs on the Navier-Stokes equations will be our future research direction.

## Acknowledgments

Research partially funded by Programma Operativo FEDER Andalucia 2014-2020 grant US-1254587 and by H2020-MSCA-RISE-2019 Project 872442 (ARIA).

## References

- [1] K. Afanasiev and M. Hinze. Adaptive control of a wake flow using proper orthogonal decomposition. *Lecture Notes in Pure and Applied Mathematics*, 216:317–332, 2001.
- [2] H. Antil, M. Heinkenschloss, and D. C. Sorensen. Application of the discrete empirical interpolation method to reduced order modeling of nonlinear and parametric systems. In *Reduced order methods for modeling and computational reduction*, pages 101–136. Springer, 2014.
- [3] M. Azaiez, T. C. Rebollo, and S. Rubino. A cure for instabilities due to advection-dominance in pod solution to advection-diffusion-reaction equations. *Journal of Computational Physics*, 425:109916, 2021.
- [4] F. Ballarin, A. Manzoni, A. Quarteroni, and G. Rozza. Supremizer stabilization of POD–Galerkin approximation of parametrized steady incompressible Navier–Stokes equations. *Int. J. Numer. Meth. Engng.*, 102:1136–1161, 2015.
- [5] H. T. Banks, R. C. del Rosario, and R. C. Smith. Reduced order model feedback control design: Computational studies for thin cylindrical shells. Technical report, North Carolina State University. Center for Research in Scientific Computation, 1998.
- [6] H. T. Banks, M. L. Joyner, B. Wincheski, and W. P. Winfree. Nondestructive evaluation using a reduced-order computational methodology. *Inverse Problems*, 16(4):929, 2000.
- [7] M. Bergmann, C.-H. Bruneau, and A. Iollo. Enablers for robust pod models. *Journal of Computational Physics*, 228(2):516–538, 2009.
- [8] T. Chacón Rebollo, E. Delgado Ávila, and M. M. Gómez Mármol. Reduced basis method for the Smagorinsky model. *Recent developments in numerical methods for model reduction (2016)*, 2016.
- [9] P. Chen, A. Quarteroni, and G. Rozza. Multilevel and weighted reduced basis method for stochastic optimal control problems constrained by stokes equations. *Numerische Mathematik*, 133(1):67–102, 2016.
- [10] D. T. Crommelin and A. J. Majda. Strategies for model reduction: comparing different optimal bases. *J. Atmos. Sci.*, 61:2206–2217, 2004.
- [11] Z. Drmac and S. Gugercin. A new selection operator for the discrete empirical interpolation method—improved a priori error bound and extensions. *SIAM Journal on Scientific Computing*, 38(2):A631–A648, 2016.
- [12] H. Fareed and J. R. Singler. A note on incremental POD algorithms for continuous time data. *arXiv preprint arXiv:1807.00045*, 2018.
- [13] U. Fernandez-Gamiz, M. Gomez-Mármol, and T. Chacón-Rebollo. Computational modeling of gurney flaps and microtabs by pod method. *Energies*, 11(8):2091, 2018.
- [14] K. Fukunaga. *Introduction to statistical pattern recognition*. elsevier academic press. san diego, san francisco, new york. 1990.

[15] M. Gunzburger, N. Jiang, and M. Schneier. An ensemble-proper orthogonal decomposition method for the nonstationary Navier-Stokes equations. *SIAM J. Numer. Anal.*, 55(1):286–304, 2017.

[16] J. S. Hesthaven, G. Rozza, and B. Stamm. *Certified Reduced Basis Methods for Parametrized Partial Differential Equations*. Springer, 2015.

[17] P. Holmes, J. L. Lumley, and G. Berkooz. *Turbulence, Coherent Structures, Dynamical Systems and Symmetry*. Cambridge, 1996.

[18] P. Holmes, J. L. Lumley, G. Berkooz, and C. W. Rowley. *Turbulence, Coherent Structures, Dynamical Systems and Symmetry, second edition*. Cambridge university press, 2012.

[19] T. Iliescu and Z. Wang. Are the snapshot difference quotients needed in the proper orthogonal decomposition? *SIAM J. Sci. Comput.*, 36(3):A1221–A1250, 2014.

[20] A. Iollo, S. Lanteri, and J.-A. Désidéri. Stability properties of pod–galerkin approximations for the compressible navier–stokes equations. *Theoretical and Computational Fluid Dynamics*, 13(6):377–396, 2000.

[21] K. Kean and M. Schneier. Error analysis of supremizer pressure recovery for pod based reduced-order models of the time-dependent navier–stokes equations. *SIAM Journal on Numerical Analysis*, 58(4):2235–2264, 2020.

[22] B. Koc, M. Mohebujjaman, C. Mou, and T. Iliescu. Commutation error in reduced order modeling of fluid flows. *Adv. Comput. Math.*, 45(5-6):2587–2621, 2019.

[23] B. Koc, S. Rubino, M. Schneier, J. Singler, and T. Iliescu. On optimal pointwise in time error bounds and difference quotients for the proper orthogonal decomposition. *SIAM Journal on Numerical Analysis*, 59(4):2163–2196, 2021.

[24] K. Kunisch and S. Volkwein. Control of the burgers equation by a reduced-order approach using proper orthogonal decomposition. *Journal of optimization theory and applications*, 102(2):345–371, 1999.

[25] K. Kunisch and S. Volkwein. Galerkin proper orthogonal decomposition methods for parabolic problems. *Numerische mathematik*, 90(1):117–148, 2001.

[26] K. Kunisch and S. Volkwein. Galerkin proper orthogonal decomposition methods for parabolic problems. *Numer. Math.*, 90(1):117–148, 2001.

[27] K. Kunisch and S. Volkwein. Galerkin proper orthogonal decomposition methods for a general equation in fluid dynamics. *SIAM Journal on Numerical analysis*, 40(2):492–515, 2002.

[28] X. Li, Y. Luo, and M. Feng. An efficient chorin-temam projection proper orthogonal decomposition based reduced-order model for nonstationary stokes equations. *arXiv preprint arXiv:2201.07398*, 2022.

[29] S. Locke and J. Singler. New proper orthogonal decomposition approximation theory for pde solution data. *SIAM Journal on Numerical Analysis*, 58(6):3251–3285, 2020.

- [30] H. V. Ly and H. T. Tran. Modeling and control of physical processes using proper orthogonal decomposition. *Mathematical and computer modelling*, 33(1-3):223–236, 2001.
- [31] C. Mou, B. Koc, O. San, L. G. Rebholz, and T. Iliescu. Data-driven variational multiscale reduced order models. *Computer Methods in Applied Mechanics and Engineering*, 373:113470, 2021.
- [32] B. R. Noack, M. Morzynski, and G. Tadmor. *Reduced-Order Modelling for Flow Control*, volume 528. Springer Verlag, 2011.
- [33] S. Perotto, A. Reali, P. Rusconi, and A. Veneziani. HIGAMod: A Hierarchical IsoGeometric Approach for MODel reduction in curved pipes. *Comput. & Fluids*, 142:21–29, 2017.
- [34] A. Quarteroni, A. Manzoni, and F. Negri. *Reduced Basis Methods for Partial Differential Equations: An Introduction*, volume 92. Springer, 2015.
- [35] A. Quarteroni, G. Rozza, et al. *Reduced order methods for modeling and computational reduction*, volume 9. Springer, 2014.
- [36] T. C. Rebollo, E. D. Aévala, M. G. Márquez, F. Ballarin, and G. Rozza. On a certified Smagorinsky reduced basis turbulence model. *SIAM J. Numer. Anal.*, 55(6):3047–3067, 2017.
- [37] T. C. Rebollo and R. Lewandowski. *Mathematical and numerical foundations of turbulence models and applications*. Springer, 2014.
- [38] C. W. Rowley. Model reduction for fluids, using balanced proper orthogonal decomposition. *International Journal of Bifurcation and Chaos*, 15(03):997–1013, 2005.
- [39] G. Rozza and K. Veroy. On the stability of the reduced basis method for Stokes equations in parametrized domains. *Comput. Methods Appl. Mech. Engrg.*, 196(7):1244–1260, 2007.
- [40] S. Rubino. A streamline derivative pod-rom for advection-diffusion-reaction equations. *ESAIM: Proceedings and Surveys*, 64:121–136, 2018.
- [41] T. P. Sapsis and P. F. J. Lermusiaux. Dynamically orthogonal field equations for continuous stochastic dynamical systems. *Phys. D*, 238(23-24):2347–2360, 2009.
- [42] R. Řeřeháček, A. Sandu, and I. M. Navon. POD/DEIM reduced-order strategies for efficient four dimensional variational data assimilation. *J. Comput. Phys.*, 295:569–595, 2015.
- [43] K. Taira, M. S. Hemati, S. L. Brunton, Y. Sun, K. Duraisamy, S. Bagheri, S. T. M. Dawson, and C.-A. Yeh. Modal analysis of fluid flows: Applications and outlook. *AIAA J.*, pages 1–25, 2019.
- [44] S. Volkwein. Proper orthogonal decomposition: Theory and reduced-order modelling. *Lecture Notes, University of Konstanz*, 2013. <http://www.math.uni-konstanz.de/numerik/personen/volkwein/teaching/POD-Book.pdf>.
- [45] J. Weller, E. Lombardi, M. Bergmann, and A. Iollo. Numerical methods for low-order modeling of fluid flows based on pod. *International Journal for Numerical Methods in Fluids*, 63(2):249–268, 2010.